

SUBSONIC WALL INTERFERENCE CORRECTIONS FOR FINITE-LENGTH
TEST SECTIONS USING BOUNDARY PRESSURE MEASUREMENTS

M. Mokry
High Speed Aerodynamics Laboratory
National Aeronautical Establishment
National Research Council Canada
Ottawa, Ontario
K1A 0R6

SUMMARY

Subsonic wall interference corrections are evaluated using the Fourier solution for the Dirichlet problem in a circular cylinder, interior to the three-dimensional test section. The required boundary values of the streamwise component of wall interference velocity are obtained from pressure measurements by a few static pressure tubes (pipes) located on the cylinder surface. The coefficients of the resultant Fourier-Bessel series are obtained in closed form and the coefficients of the Fourier sine series are calculated by the fast Fourier transform, so that the method is very efficient and suitable for routine tunnel testing. A practical use of the method is demonstrated on a theoretical example and typical model tests performed in the NAE 5 ft. \times 5 ft. wind tunnel.

NOMENCLATURE

a_n, b_n	Fourier components of u
\hat{a}_n, \hat{b}_n	boundary values of a_n, b_n
$A_{n,k}, B_{n,k}$	coefficients of Fourier sine series
C_L	lift coefficient of the model
C_p	pressure coefficient
C_y, C_z	y and z components of C_L
D_n	differential operator
f_n	common notation for a_n and b_n
\hat{f}_n	common notation for \hat{a}_n and \hat{b}_n
$F_{n,k}$	common notation for $A_{n,k}$ and $B_{n,k}$
I_n	modified Bessel function of the first kind of order n
$j_{n,k}$	k th positive zero of J_n
J_n	Bessel function of the first kind of order n
K_n	modified Bessel function of the second kind of order n
m	integer power of 2, number of equal subdivisions of interval
M_∞	stream Mach number
n	index of the Fourier component
$P_{n,k}, Q_{n,k}$	coefficients of the Fourier-Bessel series
q	dummy variable of integration
p_∞	upstream reference pressure
p_{plenum}	plenum pressure
r	radius of the control cylinder
r_m	model radius
r_s	sting radius
s	reduced test section length
S	reference area of the model
u, v, w	reduced components of wall interference velocity

U_{∞}	stream velocity
V	volume of the model
x, y, z	Cartesian co-ordinates
x, ρ, θ	cylindrical co-ordinates
x_1, x_2	x co-ordinates of the upstream and downstream ends of the control cylinder
x_N, x_T	x co-ordinates of the source and sink, representing the model
β	$(1 - M_{\infty}^2)^{1/2}$
γ	vortex strength
ΔM_{∞}	Mach number correction
ΔU_{∞}	velocity correction
$\Delta \alpha_y, \Delta \alpha_z$	correction to flow angle in the x, y and x, z planes
θ_0	angle between the lift force and y axis
κ	ratio of specific heats
μ	doublet strength
$\mu_k, \nu_{n,k}$	eigenvalues
ξ	reduced x co-ordinate
ρ_{∞}	upstream density
σ	source strength
σ_{μ}	strength of the source-sink combination
ϕ	disturbance velocity potential
ϕ_F	"free air" part of ϕ
ϕ_W	"wall interference" part of ϕ

INTRODUCTION

The present paper extends the subsonic wall correction method of Mokry and Ohman¹ to the three-dimensional case. The theoretical part of the paper has earlier been reported in Reference 2. Merits of a method that utilizes boundary pressure measurements but does not require knowledge of the cross-flow properties of ventilated test section walls are discussed in References 3 and 4. In essence, the relationship between the normal velocity and pressure difference across the wall is highly nonlinear, depending upon the boundary layer development on the wall and the pressure field induced by the model. The utilization of the measured wall static pressures as the (Dirichlet) boundary condition eliminates the need for a theoretical crossflow model, and thus indirectly ensures that the true nonlinear character of the ventilated wall is properly taken into account. However, since the acquisition of wall static pressures is required for each tunnel test; while the crossflow properties of the wall remain unknown, this approach is suitable as a post-test assessment, but not as prediction.

In contrast to some recent techniques³⁻⁶, relying upon detailed computation of flow past a model both in the wind tunnel and free air, the present paper describes an inexpensive, engineering-type estimation of wall corrections for routine tunnel testing. It is based upon the classical, linear wall interference concept, representing the model by singularities, deduced from the model geometry and measured forces⁷. The validity of this approach may be disputed⁶, but it should always be possible to compare a sample of the results with those obtained by the more elaborate techniques³⁻⁶, to decide whether in the circumstances the simple correction method is adequate or not. In many instances the corrections turn out to be marginal⁵, so that routine use of flow computation techniques is not justified.

The estimation of the far field disturbance due to the model by singularities allows to extract the axial component of wall interference velocity on the test section boundary from the measured wall static pressures. The velocity correction at the model position is obtained by solving the Dirichlet problem for the axial velocity in the test section interior. The normal components of interference velocity (incidence and sideslip corrections) are derived from the zero vorticity condition. However, since it is impractical to measure the pressures over the whole wall surfaces, a simpler solution, based on the circular cylinder interior to the test section, is proposed. The pressures are measured only by two or four static pressure tubes (pipes) on the surface of the control cylinder. Using the periodicity condition, the surface distribution of the axial component of the wall interference velocity is approximated by a Fourier expansion of axisymmetric functions. The values of Fourier components on the upstream and downstream ends of the cylinder are obtained by a "tailored" interpolation that allows a closed-form solution for the coefficients of the resultant Fourier-Bessel series. This type of solution treats the effects of blockage and lift interference separately, providing agreement with the theory of Baldwin et al⁹ and Wright¹⁰ of an infinite cylinder test section. The coefficients of the Fourier sine series are, as in the two-dimensional case¹, calculated by the fast Fourier transform, that makes the method very efficient and suitable for routine wind tunnel testing.

This simplified treatment is well justified by the fact that the three-dimensional interference is, due to the nature of propagation of pressure disturbances in space, much less severe than the two-dimensional interference. However, since the static pressure tubes are likely to be attached to the walls or mounted in their vicinity (to be outside wall boundary layers), the circular cylinder modeling restricts the application of the method to circular, octagonal or square cross-sections, as illustrated in Figure 1. The solution for the elliptic cylinder, that would allow a similar treatment of more general cross-sections, has not been worked out yet, although this should not be prohibitively difficult¹¹. For half-model tests the reflection principle has to be taken into consideration, so that the test section shapes in Figure 1 are no longer appropriate for the application of the method in its present version. For a possible estimation of the corrections for the general rectangular cross-sections, the reader is referred to References 7 and 8.

GOVERNING EQUATIONS

The model is located at the origin $x = y = 0$ of the (right-handed) Cartesian system, where x is the co-ordinate along the streamwise oriented wind tunnel axis, Figure 2. The flow is investigated in the region $x_1 < x < x_2$, $0 \leq \rho < r$, using the cylindrical co-ordinates

$$x, \rho = (y^2 + z^2)^{1/2}, \theta = \text{atan} \frac{z}{y} \quad (1)$$

It is assumed that the model is small, the incident stream is subsonic and that the disturbance velocity potential $\phi = \phi(x, \rho, \theta)$ satisfies near the cylinder boundary the linearized equation

$$\beta^2 \frac{\partial^2 \phi}{\partial x^2} + \frac{1}{\rho} \frac{\partial}{\partial \rho} \left(\rho \frac{\partial \phi}{\partial \rho} \right) + \frac{1}{\rho^2} \frac{\partial^2 \phi}{\partial \theta^2} = 0 \quad (2)$$

According to small disturbance theory, the pressure coefficient at $\rho = r$, relates to ϕ as

$$C_p(x, r, \theta) = -2 \frac{\partial \phi}{\partial x}(x, r, \theta) \quad (3)$$

However, since the measuring device — the pressure tube — is in fact a slender body, see Figure 3, the quadratic crossflow velocity components should also be retained in Equation (3). They are omitted here for the sake of linearity and no attempt is made to analyze the error.

In the linearized flow region, that is in the region of validity of Equation (2), we can use the decomposition

$$\phi(x, \rho, \theta) = \phi_F(x, \rho, \theta) + \phi_W(x, \rho, \theta) \quad (4)$$

The potential ϕ_F satisfies Equation (2) in the linearized flow region and in the exterior of the control cylinder and obeys, except in the vicinity of the vortex wake, the farfield condition

$$\phi_F \rightarrow 0 \text{ as } x^2 + (\beta\rho)^2 \rightarrow \infty$$

Near the cylinder boundary, ϕ_F can be approximated as

$$\phi_F(x, \rho, \theta) = \frac{\gamma}{4\pi} \frac{\cos(\theta - \theta_0)}{\rho} \left\{ 1 + \frac{x}{[x^2 + (\beta\rho)^2]^{1/2}} \right\} - \frac{\sigma}{4\pi} \frac{x}{[x^2 + (\beta\rho)^2]^{1/2}} + \frac{\mu}{4\pi} \frac{x}{[x^2 + (\beta\rho)^2]^{3/2}} \quad (5)$$

where θ_0 is the angle between the lift force* and the y axis.

The first term of Equation (5), the horseshoe vortex, represents the lift effect of the model. Its strength is

$$\gamma = \frac{1}{2} SC_L \quad (6)$$

The second term, the source, represents the displacement effect of the sting. Assuming that the downstream portion of the sting is a cylinder of radius r_s , the source strength is

$$\sigma = \pi r_s^2 \quad (7)$$

The last term of Equation (5), the doublet, represents the displacement effect of the test model. As shown by Baranoff¹², the strength of a three-dimensional doublet is not affected by compressibility, so that directly

$$\mu = V \quad (8)$$

For improved representation of the far field of an elongated body (missile etc.), we can replace the doublet term by the source-sink combination

*Model force normal to the x axis

$$-\frac{\sigma_\mu}{4\pi} \left\{ \frac{1}{[(x-x_N)^2 + (\beta\rho)^2]^{1/2}} - \frac{1}{[(x-x_T)^2 + (\beta\rho)^2]^{1/2}} \right\}$$

where $x_N < 0$ is the location of the nose source and $x_T > 0$ that of the tail sink, as illustrated in Figure 4. An approximate value of the strength σ_μ is

$$\sigma_\mu = \frac{\mu}{x_T - x_N}$$

In the limit $x_N, x_T \rightarrow 0$ we recover the original doublet term and for a long cylindrical body of radius r_m we obtain

$$\sigma_\mu = \pi r_m^2$$

which is also the expected limit for the source (or sink) strength, cf. Equation (7).

As shown by Hackett et al¹³, a large variety of axisymmetric bodies can be generated by the source-sink plus source combinations, so that more refined body representations for wall interference purposes seem unnecessary. However, further work is needed to find suitable far field representations for slender bodies at high angles of attack.

The potential ϕ_w satisfies Equation (2) inside the cylinder $x_1 < x < x_2$, $0 \leq \rho < r$. The derivatives of ϕ_w with respect to x , y and z determine the wall interference corrections to the components of unit wind tunnel velocity. Their evaluation at the position of the model, $x = \rho = 0$, is the subject of the next sections.

FOURIER SOLUTION OF THE WALL INTERFERENCE PROBLEM

Using the transformation

$$\xi = \frac{1}{\beta} (x - x_1) \quad (9)$$

the left-hand side of Equation (2) reduces to the Laplacian in cylindrical co-ordinates. The axial velocity function

$$u(\xi, \rho, \theta) = \frac{\partial \phi_w}{\partial \xi} (x, \rho, \theta) = \beta \frac{\partial \phi_w}{\partial x} (x, \rho, \theta) \quad (10)$$

then satisfies the equation

$$\frac{\partial^2 u}{\partial \xi^2} + \frac{1}{\rho} \frac{\partial}{\partial \rho} \left(\rho \frac{\partial u}{\partial \rho} \right) + \frac{1}{\rho^2} \frac{\partial^2 u}{\partial \theta^2} = 0 \quad (11)$$

in the region $0 < \xi < s$, $0 \leq \rho < r$, where

$$s = \frac{1}{\beta} (x_2 - x_1) \quad (12)$$

From Equations (3), (4), (9) and (10) the values of the axial component of wall interference velocity on the boundary is obtained as

$$u(\xi, r, \theta) = -\beta \left[\frac{1}{2} C_p(x, r, \theta) + \frac{\partial \phi_F}{\partial x} (x, r, \theta) \right] \quad (13)$$

Utilizing the periodicity of u and $\partial u / \partial \theta$ with respect to θ , we represent u in terms of the Fourier series

$$u(\xi, \rho, \theta) = a_0(\xi, \rho) + \sum_{n=1}^{\infty} [a_n(\xi, \rho) \cos n\theta + b_n(\xi, \rho) \sin n\theta] \quad (14)$$

where, by Equation (11)

$$\begin{aligned} D_n a_n(\xi, \rho) &= 0, \quad n = 0, 1, 2, \dots \\ D_n b_n(\xi, \rho) &= 0, \quad n = 1, 2, \dots \end{aligned} \quad (15)$$

and

$$D_n = \frac{\partial^2}{\partial \xi^2} + \frac{\partial^2}{\partial \rho^2} + \frac{1}{\rho} \frac{\partial}{\partial \rho} - \frac{n^2}{\rho^2} \quad (16)$$

The actual number of Fourier components we are able to exploit is given by the number of static pressure tubes. Thus for two tubes located at $\theta = \frac{\pi}{2}$ and $\frac{3}{2}\pi$ we have

$$u(\xi, \rho, \theta) = a_0(\xi, \rho) + b_1(\xi, \rho) \sin \theta \quad (17a)$$

and for four tubes at $\theta = 0, \frac{\pi}{2}, \pi, \frac{3}{2}\pi$, see Figure 2,

$$u(\xi, \rho, \theta) = a_0(\xi, \rho) + a_1(\xi, \rho) \cos \theta + b_1(\xi, \rho) \sin \theta + a_2(\xi, \rho) \cos 2\theta \quad (17b)$$

In order to solve for the Fourier components inside the cylinder, we introduce the boundary values

$$\begin{aligned} \hat{a}_n(\xi) &= a_n(\xi, r) \\ \hat{b}_n(\xi) &= b_n(\xi, r) \end{aligned} \quad (18)$$

and express them in terms of the known values $u(\xi, r, \theta)$, Equation (13). For the two-tube arrangement it follows from Equation (17a)

$$\begin{aligned} \hat{a}_0(\xi) &= \frac{1}{2} [u(\xi, r, \frac{\pi}{2}) + u(\xi, r, \frac{3}{2}\pi)] \\ \hat{b}_1(\xi) &= \frac{1}{2} [u(\xi, r, \frac{\pi}{2}) - u(\xi, r, \frac{3}{2}\pi)] \end{aligned} \quad (19a)$$

and for the four-tube arrangement from Equation (17b)

$$\begin{aligned} \hat{a}_0(\xi) &= \frac{1}{4} [u(\xi, r, 0) + u(\xi, r, \frac{\pi}{2}) + u(\xi, r, \pi) + u(\xi, r, \frac{3}{2}\pi)] \\ \hat{a}_1(\xi) &= \frac{1}{2} [u(\xi, r, 0) - u(\xi, r, \pi)] \\ \hat{b}_1(\xi) &= \frac{1}{2} [u(\xi, r, \frac{\pi}{2}) - u(\xi, r, \frac{3}{2}\pi)] \\ \hat{a}_2(\xi) &= \frac{1}{4} [u(\xi, r, 0) - u(\xi, r, \frac{\pi}{2}) + u(\xi, r, \pi) - u(\xi, r, \frac{3}{2}\pi)] \end{aligned} \quad (19b)$$

Using Equations (15), we now can set up the following boundary value problem

$$\begin{aligned} D_n f_n(\xi, \rho) &= 0, & 0 < \xi < s, & 0 \leq \rho < r \\ f_n(\xi, r) &= \hat{f}_n(\xi), & 0 < \xi < s \\ f_n(0, \rho) &= \hat{f}_n(0) \left(\frac{\rho}{r}\right)^n, & 0 \leq \rho < r \\ f_n(s, \rho) &= \hat{f}_n(s) \left(\frac{\rho}{r}\right)^n, & 0 \leq \rho < r \end{aligned} \quad (20)$$

where f_n is used as a common notation for both a_n and b_n .

Applying the method of separation of variables, see Reference 2, the solution is obtained in terms of a Fourier series in ξ and Fourier-Bessel series in ρ :

$$f_n(\xi, \rho) = \sum_{k=1}^{\infty} F_{n,k} \frac{I_n(\mu_k \rho)}{I_n(\mu_k r)} \sin \mu_k \xi + \sum_{k=1}^{\infty} \left[P_{n,k} \frac{\sinh \nu_{n,k}(s-\xi)}{\sinh \nu_{n,k}s} + Q_{n,k} \frac{\sinh \nu_{n,k}\xi}{\sinh \nu_{n,k}s} \right] J_n(\nu_{n,k}\rho) \quad (21)$$

where

$$\begin{aligned} \mu_k &= \frac{k\pi}{s} \\ \nu_{n,k} &= \frac{j_{n,k}}{r} \end{aligned} \quad (22)$$

and $j_{n,k}$ denotes the k th positive root of the equation $J_n(\rho) = 0$. Since

$$J_n'(\rho) = \frac{n}{\rho} J_n(\rho) - J_{n+1}(\rho)$$

the roots are easily generated by Newton's method. The first 15 values of $j_{0,k}$ and $j_{1,k}$, needed for the theoretical example below, are listed in Table 1.

The boundary values are incorporated in the coefficients

$$\begin{aligned}
 F_{n,k} &= \frac{2}{s} \int_0^s \hat{f}_n(\xi) \sin \mu_k \xi \, d\xi \\
 P_{n,k} &= \frac{2}{r^2 J_{n+1}^2(\nu_{n,k} r)} \int_0^r \hat{f}_n(0) \left(\frac{\rho}{r}\right)^n J_n(\nu_{n,k} \rho) \rho \, d\rho \\
 &= \frac{2}{\nu_{n,k} r J_{n+1}(\nu_{n,k} r)} \hat{f}_n(0) \\
 Q_{n,k} &= \frac{2}{\nu_{n,k} r J_{n+1}(\nu_{n,k} r)} \hat{f}_n(s)
 \end{aligned} \tag{23}$$

It may be noted that the closed form integration of the Fourier-Bessel coefficients in the above formulas is due to employing the factor $(\rho/r)^n$ in the interpolation of the boundary values on cylinder ends, Equations (20). The coefficients of the Fourier sine series can be evaluated, as has been done in the two-dimensional case¹, by the fast Fourier transform:

$$F_{n,k} = \frac{2}{m} \sum_{j=0}^{m-1} \hat{f}_n(s) \frac{2j+1}{m} \sin \frac{2\pi j k}{m}, \quad k = 1, 2, \dots, m/2-1 \tag{24}$$

where m is an integer power of 2 and the discrete values of \hat{f}_n are obtained using the odd extension of the boundary function $\hat{f}_n(\xi)$ on the interval $0 < \xi < 2s$. Accordingly, the Fourier sine series of Equation (21) is truncated to the first $m/2-1$ terms. For consistency, the same number of terms is also used for the truncated Fourier-Bessel series.

WALL INTERFERENCE CORRECTIONS

Having constructed the velocity function (14), we can proceed to evaluate the velocity and Mach number corrections. The correction to stream velocity U_∞ applicable at the model position, is

$$\Delta U_\infty = U_\infty \frac{\partial \phi_W}{\partial x}(0,0,\theta) \tag{25}$$

where from Equations (9) and (10)

$$\frac{\partial \phi_W}{\partial x}(0,0,\theta) = \frac{1}{\beta} u\left(-\frac{x_1}{\beta}, 0, \theta\right) \tag{26}$$

Using Equations (14), (21) and (23), the required axial value

$$\begin{aligned}
 u(\xi, 0, \theta) &= \sum_{k=1}^{m/2-1} A_{0,k} \frac{\sin \mu_k \xi}{I_0(\mu_k r)} \\
 &+ \sum_{k=1}^{m/2-1} \left[\hat{a}_0(0) \frac{\sinh \nu_{0,k}(s-\xi)}{\sinh \nu_{0,k} s} + \hat{a}_0(s) \frac{\sinh \nu_{0,k} \xi}{\sinh \nu_{0,k} s} \right] \frac{2}{\nu_{0,k} r J_1(\nu_{0,k} r)}
 \end{aligned} \tag{27}$$

where, according to Equation (24)

$$A_{0,k} = \frac{2}{m} \sum_{j=0}^{m-1} \hat{a}_0(s) \frac{2j+1}{m} \sin \frac{2\pi j k}{m} \tag{28}$$

As expected from the properties of a harmonic function u , the axial correction (25) proves to be independent of angle θ . Accordingly, only the zeroth term of the Fourier expansion (14) contributes in Equation (27).

The Mach number correction is obtained from the differentiated relation between Mach number and velocity as

$$\Delta M_\infty = \left(1 + \frac{\kappa-1}{2} M_\infty^2\right) M_\infty \frac{\partial \phi_W}{\partial x}(0,0,\theta) \tag{29}$$

where the x derivative of the interference potential is given by Equation (26).

The corrections to the components of the flow angle (in radians) at the position of the model are

$$\Delta\alpha_y = \frac{\partial\phi_w}{\partial y}(0,0,\theta)$$

$$\Delta\alpha_z = \frac{\partial\phi_w}{\partial z}(0,0,\theta) \quad (30)$$

where, again, the value of θ is immaterial. As in the two-dimensional case¹, the flow angle correction can be expressed in terms of the velocity function u to within arbitrary constant terms. Integrating the total differentials of $\partial\phi_w/\partial y$ and $\partial\phi_w/\partial z$ along a path between the reference point $x = x_1, \rho = 0$ and the model position $x = \rho = 0$, we obtain

$$\frac{\partial\phi_w}{\partial y}(0,0,\theta) - \frac{\partial\phi_w}{\partial y}(x_1,0,\theta) = v(-\frac{x_1}{\beta},0,\theta) - v(0,0,\theta) \quad (23)$$

$$\frac{\partial\phi_w}{\partial z}(0,0,\theta) - \frac{\partial\phi_w}{\partial z}(x_1,0,\theta) = w(-\frac{x_1}{\beta},0,\theta) - w(0,0,\theta)$$

where

$$v(\xi,0,\theta) = \int \frac{\partial u}{\partial y}(\xi,0,\theta) d\xi \quad (24)$$

$$w(\xi,0,\theta) = \int \frac{\partial u}{\partial z}(\xi,0,\theta) d\xi$$

are the conjugate velocity functions. For the application in the above differences, the selection of the integration constant is obviously irrelevant. Using Equations (1), (21) and (23)

$$\begin{cases} v(\xi,0,\theta) \\ w(\xi,0,\theta) \end{cases} = \sum_{k=1}^{m/2-1} \begin{cases} A_{1,k} \\ B_{1,k} \end{cases} \frac{\cos \mu_k \xi}{2I_1(\mu_k r)} + \sum_{k=1}^{m/2-1} \left[\begin{cases} \hat{a}_1(0) \\ \hat{b}_1(0) \end{cases} \frac{\cosh \nu_{1,k}(s-\xi)}{\sinh \nu_{1,k} s} + \begin{cases} \hat{a}_1(s) \\ \hat{b}_1(s) \end{cases} \frac{\cosh \nu_{1,k} \xi}{\sinh \nu_{1,k} s} \right] \frac{1}{\nu_{1,k} r J_2(\nu_{1,k} r)} \quad (31)$$

where, according to Equation (24)

$$A_{1,k} = \frac{2}{m} \sum_{j=0}^{m-1} \hat{a}_1(s \frac{2j+1}{m}) \sin \frac{2\pi j k}{m}$$

$$B_{1,k} = \frac{2}{m} \sum_{j=0}^{m-1} \hat{b}_1(s \frac{2j+1}{m}) \sin \frac{2\pi j k}{m} \quad (32)$$

Using Equations (4) and (5) we finally obtain

$$\Delta\alpha_y = v(-\frac{x_1}{\beta},0,\theta) - v(0,0,\theta) + \frac{\partial\phi}{\partial y}(x_1,0,\theta) - \frac{\gamma}{8\pi} \frac{\beta^2}{x_1^2} \cos \theta_0$$

$$\Delta\alpha_z = w(-\frac{x_1}{\beta},0,\theta) - w(0,0,\theta) + \frac{\partial\phi}{\partial z}(x_1,0,\theta) - \frac{\gamma}{8\pi} \frac{\beta^2}{x_1^2} \sin \theta_0 \quad (33)$$

The flow angles $\partial\phi/\partial y$ and $\partial\phi/\partial z$ at $x = x_1, \rho = 0$ can either be measured or, if the test section is sufficiently long, set equal to the upstream flow angles, known from empty tunnel calibration.

The second derivatives $\partial^2\phi_w/\partial x^2$, $\partial^2\phi_w/\partial x\partial y$ and $\partial^2\phi_w/\partial x\partial z$, representing the pressure gradient and streamline curvature effects, are readily obtained by differentiating the series (27) and (31) with respect to ξ . For the tunnel test to be correctable by a simple adjustment in stream Mach number and flow inclination, the second (and higher) derivatives are supposed to be small.

AUTOCORRECTION PROPERTIES OF THE METHOD

As pointed out by Capelier, Chevallier and Bouniol in connection with a similar method⁷, the velocity correction compensates automatically for small errors of the reference velocity level. This is of particular importance to three-dimensional ventilated test sections, since very often as reference pressure is taken that measured in the surrounding plenum chamber. Denoting by a tilde the quantities based on the plenum pressure, p_{plenum} , we write for the boundary pressure coefficient

$$\tilde{C}_p(x,r,\theta) = C_p(x,r,\theta) - C_{p_{\text{plenum}}}$$

where

$$C_{p_{\text{plenum}}} = \frac{p_{\text{plenum}} - p_{\infty}}{\frac{1}{2} \rho_{\infty} U_{\infty}^2}$$

According to Equation (13), the boundary value of the axial velocity function is

$$\tilde{u}(\xi, r, \theta) = -\beta \left[\frac{1}{2} \tilde{C}_p(x, r, \theta) + \frac{\partial \phi_F}{\partial x}(x, r, \theta) \right] = u(\xi, r, \theta) + \frac{\beta}{2} C_{p_{\text{plenum}}}$$

By linear superposition, the solution on the tunnel axis is obtained as

$$\tilde{u}(\xi, 0, \theta) = u(\xi, 0, \theta) + \frac{\beta}{2} C_{p_{\text{plenum}}}$$

where $u(\xi, 0, \theta)$ is given by Equation (27). From small disturbance theory it also follows that the (fictitious) stream velocity corresponding to p_{plenum} is

$$\tilde{U}_{\infty} = U_{\infty} \left(1 - \frac{1}{2} C_{p_{\text{plenum}}} \right)$$

Consequently, the corrected stream velocity at the model position is

$$U_{\infty} + \Delta U_{\infty} = U_{\infty} \left[1 + \frac{1}{\beta} u \left(-\frac{x_1}{\beta}, 0, \theta \right) \right] = \tilde{U}_{\infty} \left[1 + \frac{1}{\beta} \tilde{u} \left(-\frac{x_1}{\beta}, 0, \theta \right) \right] = \tilde{U}_{\infty} + \Delta \tilde{U}_{\infty}$$

if the products of small terms are neglected. Similarly

$$M_{\infty} + \Delta M_{\infty} = \tilde{M}_{\infty} + \Delta \tilde{M}_{\infty}$$

This simple result has far reaching implications. It shows that, as long as the reference pressure does not differ from the upstream static pressure greatly, we always arrive at the same value of the corrected stream Mach number. The present method thus provides the much needed correspondence between the plenum pressure and the stream Mach number at the position of the model. As a matter of fact, each tunnel run that incorporates the wall pressure measurement qualifies as a calibration run. This also implies that the empty tunnel calibration (plenum pressure versus test section Mach number) should not be applied towards the Mach number corrected according to the present method.

THEORETICAL EXAMPLE

To show the feasibility and accuracy of the present method, a test example is first worked out for a theoretical case of an infinitely long cylindrical test section. For the solid wall boundary condition

$$\frac{\partial \phi}{\partial \rho}(x, r, \theta) = 0, \quad -\infty < x < \infty, \quad 0 \leq \theta < 2\pi$$

and ϕ_F described by Equation (5), the exact solution satisfying the upstream condition

$$\lim_{x \rightarrow -\infty} \frac{\partial \phi_W}{\partial x}(x, \rho, \theta) = 0$$

is^{9,10}

$$\begin{aligned} \phi_W = & \frac{\gamma}{4\pi} \frac{\cos(\theta - \theta_0)}{r} \left[\frac{\rho}{r} - \frac{2}{\pi} \int_0^{\infty} \frac{K_1(q) + qK_0(q)}{I_1(q) - qI_0(q)} I_1 \left(\frac{q\rho}{r} \right) \sin \left(\frac{qx}{\beta r} \right) dq \right] \\ & + \frac{\sigma}{2\pi\beta r} \left[\frac{x}{\beta r} - \frac{1}{\pi} \int_0^{\infty} \frac{K_1(q)}{I_1(q)} I_0 \left(\frac{q\rho}{r} \right) \cos \left(\frac{qx}{\beta r} \right) dq \right] \\ & + \frac{\mu}{2\pi^2(\beta r)^2} \int_0^{\infty} \frac{K_1(q)}{I_1(q)} I_0 \left(\frac{q\rho}{r} \right) q \sin \left(\frac{qx}{\beta r} \right) dq \end{aligned} \quad (34)$$

and us
-1.6 <
those
sample
can be
practic
be scal

CORR

transp
attach
angle
and (C
area,
be th
sectic
(base
is sin
porti
the a
of at

COR

again
tion
pres
they
of t
full
pre
In :
exc

CO

pre
au
Mi
ac
of

A

C

I

Selecting the values $r = 1$ (arbitrary length units, L), $M_\infty = 0.7$, $C_L = 1.0$, $\theta_o = 105^\circ$, $r_s = 0.05$ (L), $V = 0.02$ (L³), $S = 0.1$ (L²) and using Equations (3)-(5), the pressure coefficients are generated at $\theta = 0, \frac{\pi}{2}, \pi, \frac{3}{2}\pi$ and 16 equidistant points on the interval $-1.6 < x < 1.6$ (L), see Table 2. The comparison of the exact correction values, calculated from Equations (29), (30) and (34), with those obtained by the present method from the generated pressures is given in Table 3. It is seen that already such a small pressure sample as that given in Table 2 yields technically acceptable accuracy of the corrections. As shown in Reference 2, further improvement can be obtained by increasing the number of pressure points and extending the interval of x farther upstream and downstream. In practice, there are of course limits imposed by the actual physical length of the test section and the number of pressure orifices that can be scanned.

CORRECTIONS FOR AN AIRCRAFT MODEL

Figures 5a - b show pressure distributions measured by static pressure pipes above ($\theta = 90^\circ$) and below ($\theta = 270^\circ$) a transport aircraft model in the NAE 5 ft. \times 5 ft. blowdown wind tunnel. The 1 in. diameter pipes, sketched in Figure 3, are directly attached to the 20% perforated walls. Since the side force is essentially zero, two tubes are sufficient for the determination of the flow angle correction, but for a more accurate evaluation of the Mach number correction four tubes would be preferable, cf. Equations (19a) and (19b). The span of the (straight) wing is 47 in. (78% of the section span), the model volume is $V = 1100$ in.³ and the reference area, on which the force coefficients are based, is $S = 220$ in.². The point where the corrections are evaluated ($x/h = 0$) is selected to be the intersection of wing quarter-chord lines. It is seen that with respect to the pressure pipes, extending over the perforated test section length, the model is located too far downstream. In the higher incidence case, Figure 5b the upstream pressure coefficients (based on the plenum pressure) converge to zero, but in the lower incidence case, Figure 5a they tend to a slightly negative limit. This is simply an indication that the pressure established during the tunnel run in the plenum chamber is higher than that in the upstream portion of the test section. This affects the Mach number correction, but presumably not the resultant, corrected Mach number (see the autocorrection properties of the method). In both cases, Figures 5a and b, the Mach number correction is found small and the angle of attack correction negligible.

CORRECTIONS FOR A SLENDER MODEL

Figures 6a - c show pressure distributions measured by four static pressure tubes during a test of a rocket launcher model, again in the NAE 5 ft. \times 5 ft. wind tunnel. The body has diameter 6.5 in. and length 48 in.; with respect to the rails it is again positioned too far back. The forces are normalized by the circular cross-section of the body. The differences between the upstream pressures on the side tubes ($\theta = 0^\circ$ and 180°) and the top and bottom tubes ($\theta = 90^\circ$ and 270°) are puzzling, particularly since they already exist near zero incidence, see Figure 6a. Admittedly, the axial symmetry is somewhat disturbed by attachment lugs on top of the model and by the downstream influence of a vertical strut¹⁴ (neither is shown in the figures), but we are not sure if this can fully account for the effect. In Figure 6c the proximity of the model nose to the wall has a noticeable influence on the upper wall pressure and the representation of the model far field by the axial source-sink combination is questionable for such a high incidence. In any case, the evaluated Mach number correction is small at all three incidences, Figures 6a - c. The angle of attack correction is small except for the low incidence case, Figure 6a which is not impossible, but contrary to our expectations.

CONCLUSIONS

A practical method has been presented for the assessment of three-dimensional wall interference corrections from boundary pressures, measured by static pressure tubes at the test section walls, and the aerodynamic forces, acting on the model. The method is autocorrective with respect to errors of the reference pressure and provides a link between the plenum pressure and the test section Mach number. The accuracy is demonstrated on a theoretical example of the cylindrical closed wall test section. An application to actual tunnel data from a perforated wall test section shows that the corrections are rather small and that a more elaborate computation of three-dimensional wall interference effects at subcritical flow conditions at the walls seems unwarranted.

ACKNOWLEDGEMENT

The author wishes to thank J.R. Digney and F.C. Tang of the High Speed Aerodynamics Laboratory, National Research Council Canada, for providing their unpublished experimental data and helpful discussions.

REFERENCES

1. Mokry, M.
Ohman, L.H. *Application of the Fast Fourier Transform to Two-Dimensional Wind Tunnel Wall Interference.* Journal of Aircraft, Vol. 17, June 1980, pp. 402-408.
2. Mokry, M. *Evaluation of Three-Dimensional Wall Interference Corrections from Boundary Pressure Measurements.* LTR-HA-51, National Aeronautical Establishment, National Research Council Canada, November 1980.
3. Stahara, S.
Spreiter, J.R. *Transonic Wind Tunnel Interference Assessment - Axisymmetric Flows.* AIAA Journal, Vol. 18, 1980, pp. 63-71.
4. Hinson, B.L.
Burdges, K.P. *Acquisition and Application of Transonic Wing and Far-Field Test Data for Three-Dimensional Computational Method Evaluation.* AFOSR-TR-80-0421, Lockheed-Georgia Co., March 1980.
5. Mercer, J.E.
Geller, E.W.
Johnson, M.L.
Jameson, A. *Transonic Flow Calculations for a Wing in a Wind Tunnel.* Journal of Aircraft, Vol. 18, 1981, pp. 707-711.

6. Rizk, M.H.
Hafez, M.
Murman, E.M.
Lovell, D. *Transonic Wind Tunnel Wall Interference Corrections for Three-Dimensional Models.*
AIAA Paper 82-0588, March 1982.
7. Capelier, C.
Chevallier, J.-P.
Bouniol, F. *Nouvelle méthode de correction des effets de parois en courant plan.*
La Recherche Aéronautique, January-February 1978, pp. 1-11.
8. Sawada, H. *Wind Tunnel Interference in a Test Section with Ventilated Walls.*
ICAS-80-23.5, October 1980.
9. Baldwin, B.S.
Turner, J.B.
Knechtel, E.D. *Wall Interference in Wind Tunnels with Slotted and Porous Boundaries at Subsonic Speeds.*
NACA TN 3176, May 1954.
10. Wright, R.H. *The Effectiveness of the Transonic Wind Tunnel as a Device for Minimizing Tunnel-Boundary Interference for Model Tests at Transonic Speeds.*
AGARD Rept. 294, March 1959.
11. Lotz, I. *Correction of Downwash in Wind Tunnels of Circular and Elliptic Sections.*
NACA TM 801, July 1936.
12. v.Baranoff, A. *Tunnel Corrections for Compressible Subsonic Flow.*
NACA TM 1162, July 1947.
13. Hackett, J.E.
Wilsden, D.J.
Lilley, D.E. *Estimation of Tunnel Blockage from Wall Pressure Signatures; A Review and Data Correlation.*
NASA CR-15,224, March 1979.
14. Brown, D. *Information for Users of the National Research Council's 5-ft. x 5-ft. Blowdown Wind Tunnel at the National Aeronautical Establishment, Third Ed.*
LTR-HA-6, National Aeronautical Establishment, National Research Council Canada, September 1977.

TABLE 1

ZEROS OF BESSEL FUNCTIONS J_0 AND J_1

k	$j_{0,k}$	$j_{1,k}$
1	2.40483	3.83171
2	5.52008	7.01559
3	8.65373	10.17347
4	11.79153	13.32369
5	14.93092	16.47063
6	18.07106	19.61586
7	21.21164	22.76008
8	24.35247	25.90367
9	27.49348	29.04683
10	30.63461	32.18968
11	33.77582	35.33231
12	36.91710	38.47477
13	40.05843	41.61709
14	43.19979	44.75932
15	46.34119	47.90146

TABLE 2
PRESSURE COEFFICIENTS ON THE CONTROL CYLINDER
(THEORETICAL EXAMPLE)

x	C _p			
	θ = 0	θ = π/2	θ = π	θ = 3/2π
-1.5	0.00024	-0.00115	-0.00035	0.00104
-1.3	0.00033	-0.00200	-0.00066	0.00167
-1.1	0.00034	-0.00354	-0.00130	0.00258
-0.9	-0.00001	-0.00645	-0.00273	0.00371
-0.7	-0.00154	-0.01207	-0.00599	0.00454
-0.5	-0.00607	-0.02268	-0.01309	0.00351
-0.3	-0.01553	-0.03967	-0.02573	-0.00159
-0.1	-0.02661	-0.05670	-0.03933	-0.00924
0.1	-0.02900	-0.05909	-0.04172	-0.01163
0.3	-0.02176	-0.04590	-0.03196	-0.00782
0.5	-0.01442	-0.03103	-0.02144	-0.00484
0.7	-0.01081	-0.02134	-0.01526	-0.00473
0.9	-0.00962	-0.01606	-0.01234	-0.00590
1.1	-0.00940	-0.01328	-0.01104	-0.00716
1.3	-0.00946	-0.01178	-0.01044	-0.00811
1.5	-0.00956	-0.01095	-0.01015	-0.00876

TABLE 3
WALL INTERFERENCE CORRECTIONS (THEORETICAL EXAMPLE)

	Exact	Present Method
		-1.6 < x < 1.6 m = 32
ΔM _∞	0.00724	0.00715
Δα _y (deg)	-0.05900	-0.05420
Δα _z (deg)	0.22020	0.20228
∂ΔM _∞ /∂x (1/L)	0.00210	0.00207
∂Δα _y /∂x (deg/L)	-0.08254	-0.08123
∂Δα _z /∂x (deg/L)	0.30803	0.30315

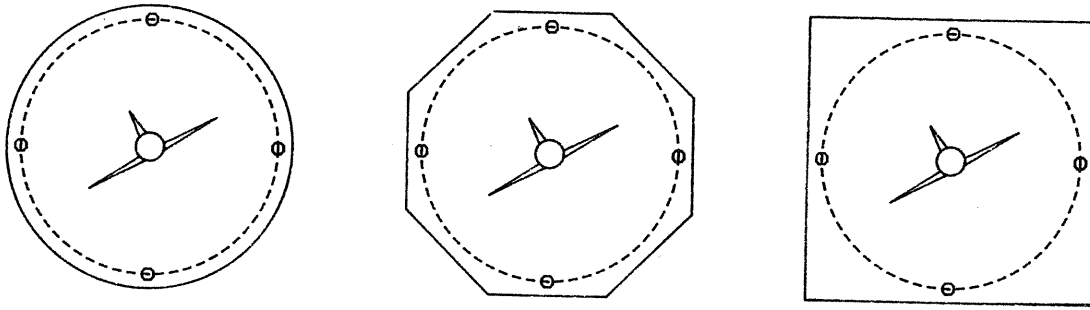


FIG. 1: POSITIONING OF STATIC PRESSURE TUBES

I, II, III, IV pressure tubes

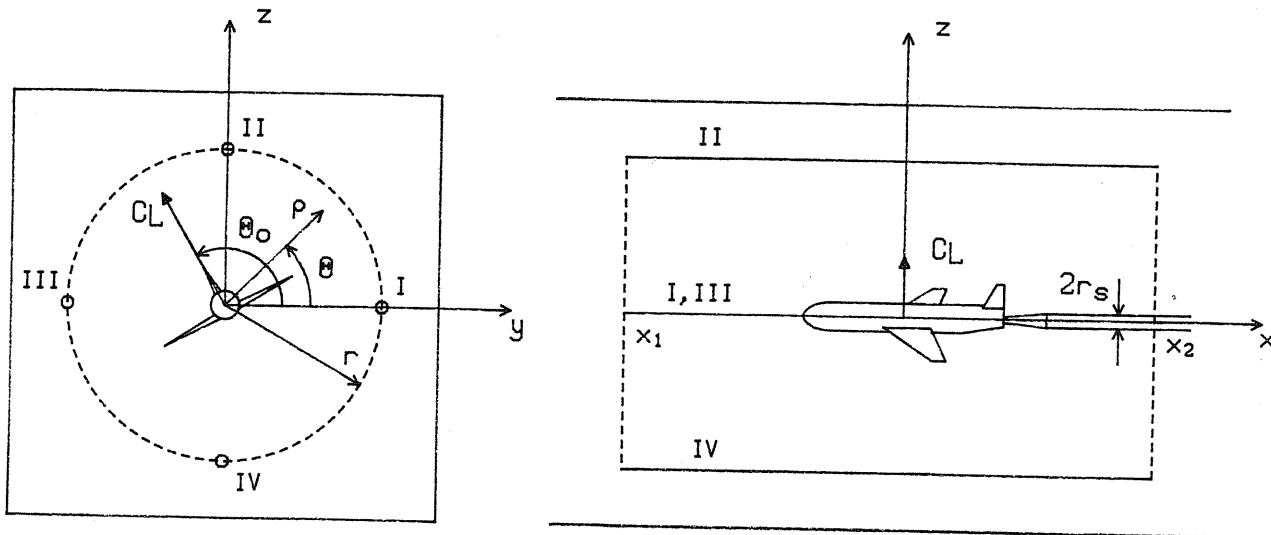


FIG. 2: CO-ORDINATE SYSTEM

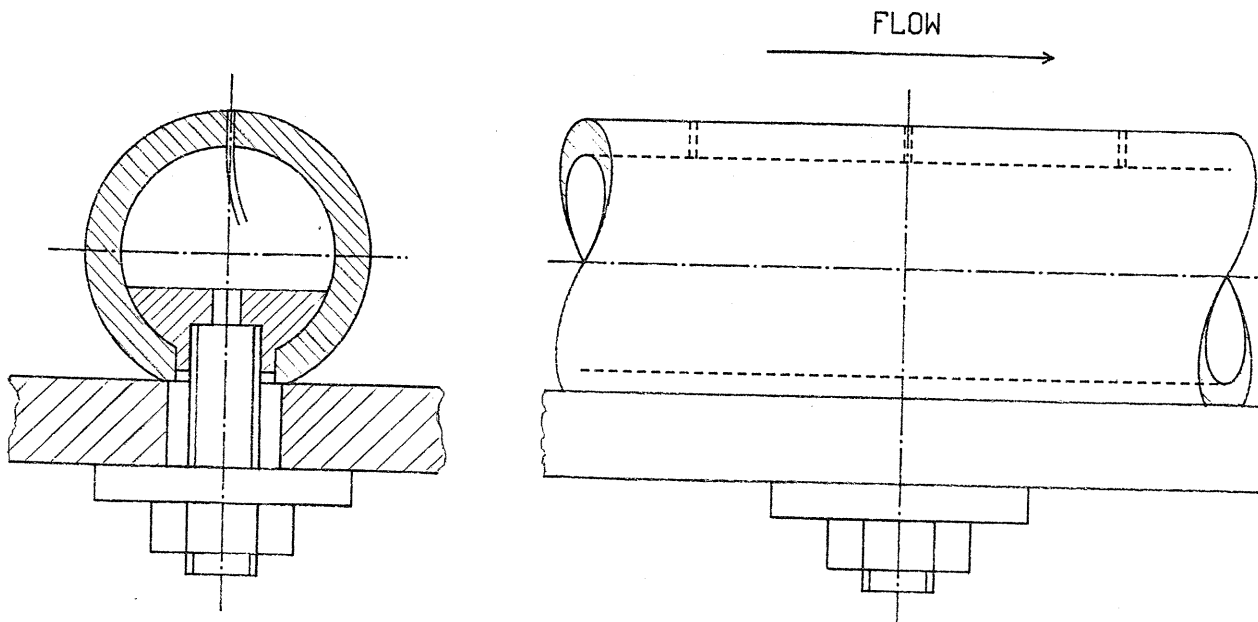


FIG. 3: DETAIL OF THE STATIC PRESSURE TUBE

Cp = -0.15

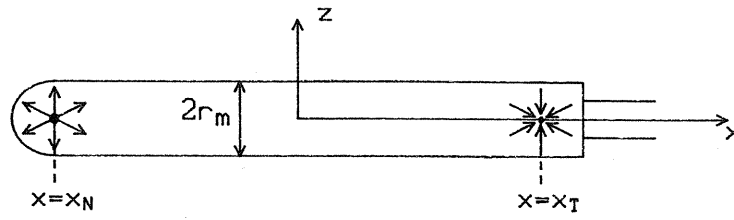


FIG. 4: SOURCE-SINK REPRESENTATION FOR AN ELONGATED BODY

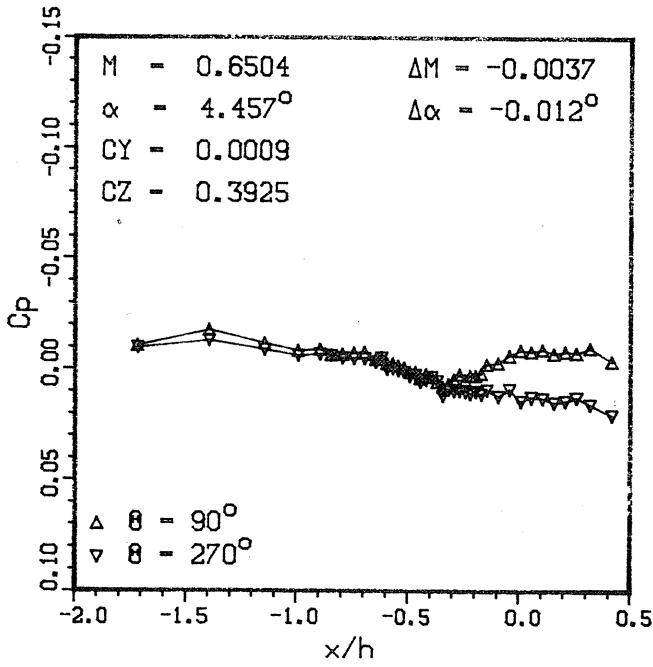


FIG. 5a: WALL PRESSURES FOR AN AIRCRAFT MODEL



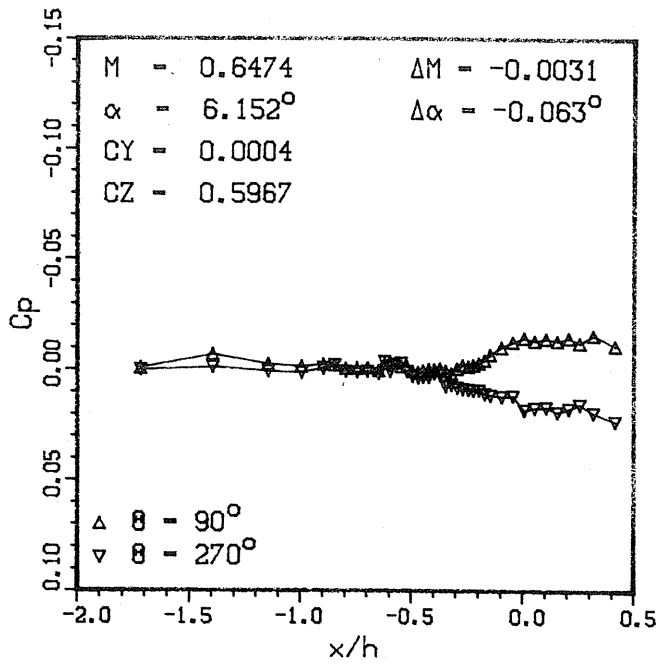


FIG. 5b: WALL PRESSURES FOR AN AIRCRAFT MODEL

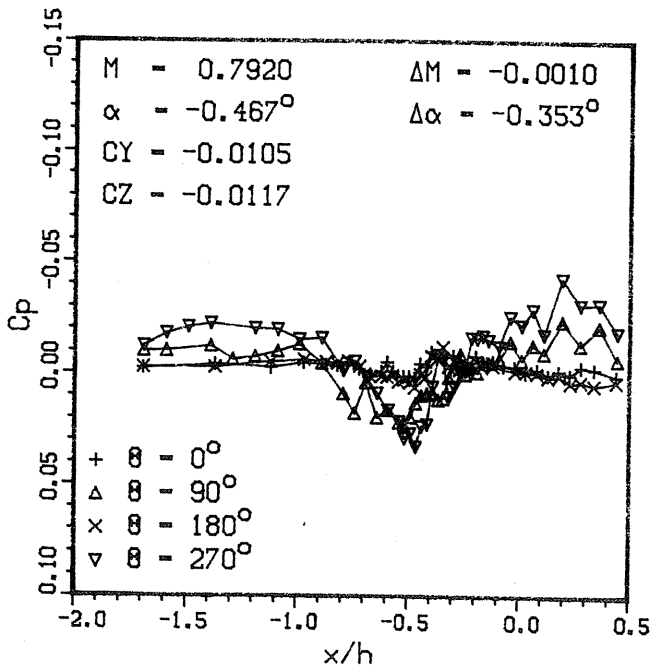
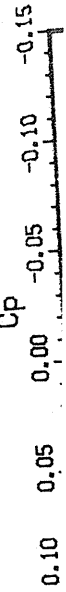
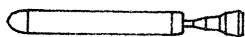


FIG. 6a: WALL PRESSURES FOR A SLENDER MODEL



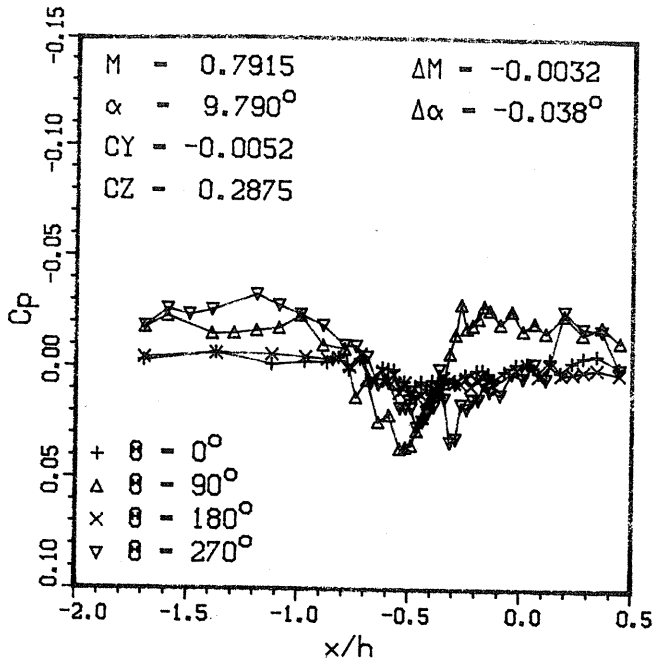


FIG. 6b: WALL PRESSURES FOR A SLENDER MODEL

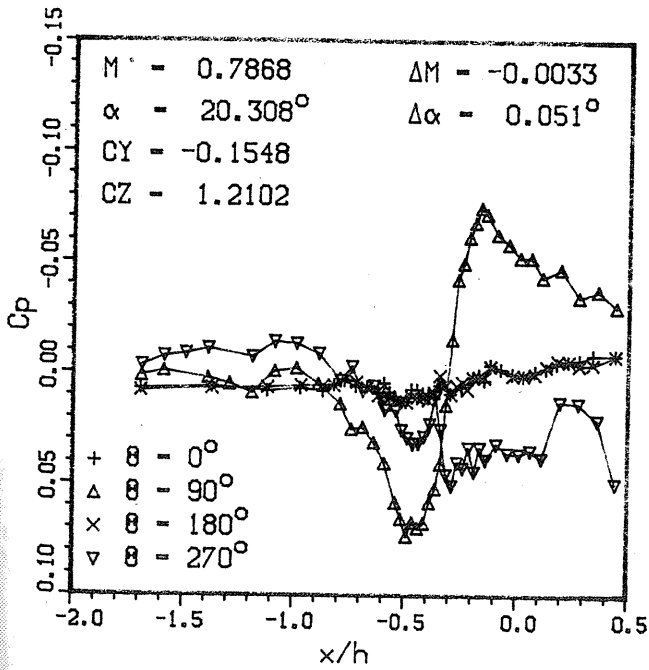
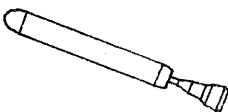


FIG. 6c: WALL PRESSURES FOR A SLENDER MODEL



DEL